Dynamical Analysis and Control of Micro-cantilevers

M. Ashhab, M.V. Salapaka, M. Dahleh and I. Mezić
Mechanical and Environmental Engineering Dept.
University of California at Santa Barbara
CA 93106

March 10, 1997

Abstract

In this paper, we study the dynamical behaviour of a microcantilever-sample system that forms the basis for the operation of atomic force microscopes (AFM). We model the micro-cantilever by a single mode approximation and the interaction between the sample and cantilever by a van der Waals (vdW) potential. The cantilver is vibrated by a sinusoidal input, and its deflection is detected optically. We analyze the forced dynamics using Melnikov method, which reveals the region in the space of physical parameters where chaotic motion is possible. In addition, using a proportional and derivative controller we compute the Melnikov function in terms of the parameters of the controller. Using this relation it is possible to design controllers that will remove the possibility of chaos.

1 Introduction

Surfaces at the atomic level can be probed with good accuracy using the atomic force microscope (AFM) which was invented in 1986. This is done by moving the sample beneath a tip attached to a soft cantilever which causes the cantilever to deflect. The cantilever deflection is measured by optical methods and is used as an indicator of the force variation on the sample. The behaviour of the cantilever depends on the interaction force between its tip and the sample, the spring force which is due to the cantilever, and the equilibrium position of the tip in the absence of the interaction forces. Many cantilever-based instruments are now available which can be used for force measurements, magnetic spin detection, and thermal measurements [10]. All of these instruments share this basic mechanism of a micro-cantilever interacting with a sample.

It has been experimentally observed that the motion of the cantilever can be chaotic under certain physical condition [11]. This type of irregular motion is highly undesirable for the AFM performance since it causes the AFM to give inaccurate measurements. This paper is concerned with the modeling, analysis and control of a typical cantilever sample interaction, which as was mentioned above is at the heart of the detection scheme employed by AFM's. The objective is to ensure good performance of the microscope by identifying and

subsequently eliminating the possibility of chaotic motion of the cantilever. In this work, we show that based on a certain model approximation of the cantilever-sample system it is possible to design controllers that will substantially improve the behaviour of the system by eliminating the possibility of chaos.

We now describe briefly the contents of this paper. In section 2, we give a multimode model approximation of the cantilever and from that we extract an approximation for the cantilever-sample model. The dynamical analysis of the forced cantilever-sample system is carried out in section 3. This section will include the analysis of the effect of feedback on the qualitative behaviour of the system, and how a controller can be implemented to eliminate the possibility of chaos in the system. Finally, we draw our conclusions in section 4.

2 Model Description

As has been stated before, the cantilever is at the heart of the detection scheme employed by the atomic force microscope. It is essential that the dynamics of the cantilever be fully understood, before attempting to unfold the complex dynamics which is introduced due to the cantilever-sample interaction.

In the first part of this section we present the analysis of the cantilever dynamics relevant for the atomic force microscope. In the second part of this section we utilize a one mode approximation of the multi-mode model developed to study the cantilever-sample interaction.

2.1 Multi-mode Model of the Cantilever

Figure 1 shows a cantilever subject to multiple loading. One end of the cantilever is fixed and the other end is free. The distributed applied load per unit length is given by $p(x,t)$. A concentrated load $F(t)$ is applied at a distance x_f from the base of the cantilever. The distributed load may be due to a piezoelectric material on the cantilever and the concentrated force may be due to the interaction between the sample and the cantilever tip. The damping force per unit length is denoted by $p_d(x,t)$. The length of the cantilever is L, its Young's modulus of elasticity is E, its cross sectional area is A, and its area moment of inertia is I (all in SI units).

2.1.1 Undamped Free Vibration

In the absence of damping and applied loads, the equation of motion of the cantilever is given by

$$EI\frac{\partial^4 z(x,t)}{\partial x^4} + \rho A\frac{\partial^2 z(x,t)}{\partial t^2} = 0,\ z(x,0) = a(x),\ \frac{\partial z(x,0)}{\partial t} = b(x), \tag{1}$$

where $a(x)$, $b(x)$ are the initial conditions of the cantilever and $z(x,t)$ is the displacement of the cantilever. We will use the convention that $f'(x,t)$ denotes the spatial derivative,

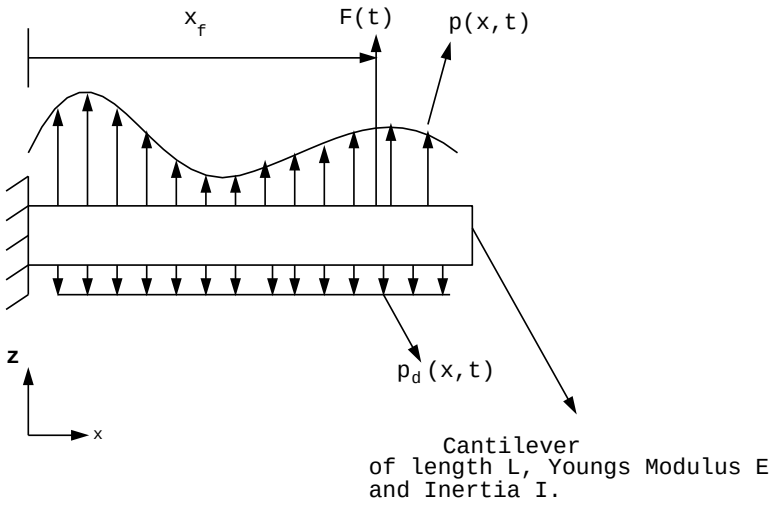

Figure 1: A schematic showing a cantilever subjected to an applied load, $p(x,t)$, the damping force, $p_d(x,t)$ assumed constant per unit length and a concentrated force $F(t)$ applied at a distance x_f from the base of the cantilever.

$\frac{\partial f(x,t)}{\partial x}$ and $\dot{f}(x,t)$ denotes the time derivative, $\frac{\partial f(x,t)}{\partial t}$. It can be shown [4] that the solution of Eq. (1) has the form

$$z(x,t) = \sum_{j=1}^{\infty} C_j \sin(\omega_j t + \delta_j)\phi_j, \tag{2}$$

with

$$\phi_j(x) = (\sin\lambda_j L + \sinh\lambda_j L)(\cos\lambda_j x - \cosh\lambda_j x) + (\cos\lambda_j L + \cosh\lambda_j L)(\sinh\lambda_j x - \sin\lambda_j x), \tag{3}$$

where λ_j is a solution of

$$\cos\lambda_j L \, \cosh\lambda_j L + 1 = 0. \tag{4}$$

The j^{th} mode deformation of the cantilever is given by $\phi_j(x)$, whereas the wavelength of the j^{th} mode is given by $\lambda_j L$. The wavelengths are arranged in an ascending order ($\lambda_1 < \lambda_2 < \ldots$). The relation between the wavelength and frequency of mode j is given by

$$(\lambda_j L)^4 = \frac{\omega_j^2 \rho A L^4}{EI}. \tag{5}$$

It can be shown that the cantilever deformations ϕ_j satisfy the relations;

$$\int_0^L \phi_j(x)\phi_k(x)dx = \delta_{kj} L I_j, \tag{6}$$

$$\int_0^L \phi_j''(x)\phi_k''(x)dx = \delta_{kj}\lambda_j^4 L I_j, \tag{7}$$

$$\int_0^L \phi_j(x)dx = -\frac{2(\cos\lambda_j L + \cosh\lambda_j L)}{\lambda_j} =: J_j, \tag{8}$$

$$\phi_j(L) = 2(\cos\lambda_j L \sinh\lambda_j L - 2\sin\lambda_j L \cosh\lambda_j L), \tag{9}$$

$$\phi_j'(L) = -2\lambda_j(\sinh\lambda_j L \sin\lambda_j L), \tag{10}$$

where $I_j = (\sin\lambda_j L + \sinh\lambda_j L)^2$, $\delta_{kj} = 0$ if $k \neq j$ and $\delta_{kj} = 1$ if $k = j$. Conveniently, $\omega_j^2 = \frac{k_j}{m_j}$ if we define

$$k_j := EI\int_0^L \phi_j''(x)\phi_j''(x)dx \text{ and } m_j := \rho A\int_0^L \phi_j(x)\phi_j(x)dx. \tag{11}$$

2.1.2 Forced Vibration with Damping

To study the dynamics of the cantilever subjected to time varying forces we apply the *principle of virtual work* to obtain the equation of motion [5]. Let the displacement of the cantilever at position x and time t be given by $z(x,t)$. Suppose the cantilever is given a virtual displacement of $\delta u(x,t)$. The elastic work and the inertial work done by the cantilever are given by [5]

$$-EI\int_0^L z''(\delta u)''dx \quad \text{and} \quad -\rho A\int_0^L \ddot{z}(x,t)\delta u(x,t)dx,$$

respectively, whereas the work done by the external applied forces and the damping force are given by

$$\int_0^L p(x,t)\delta u(x,t)dx + F\delta u(x_f,t) \quad \text{and} \quad -\int_0^L p_d(x,t)\delta u(x,t)dx,$$

respectively. Using the principle of virtual work whereby the net work must be zero, we obtain

$$\int_0^L \{-EIz''(\delta u)'' - \rho A\ddot{z}(x,t)\delta u(x,t) - p_d(x,t)\delta u(x,t) + p(x,t)\delta u(x,t)\}dx + F\delta u(x_f,t) = 0. \tag{12}$$

We assume that the damping is uniform and given by $p_d(x,t) = \xi\dot{z}(x,t)$. It can be shown that any function $r(x)$ which satisfies the boundary conditions imposed by the fixed-free cantilever defined between 0 and L can be expanded as $r(x) = \sum_{k=1}^{\infty}\phi_k(x)q_k$ where $\phi_k(x)$ were obtained from the free undamped vibration [5]. Thus, any deformation of the cantilever can be represented as a weighted combination of the fundamental mode deformations of the unforced cantilever. Therefore there exist coefficients $q_k(t)$ and $\delta u_k(t)$ such that,

$$z(x,t) = \sum_{k=1}^{\infty}\phi_k(x)q_k(t) \quad \text{and} \quad \delta u(x,t) = \sum_{k=1}^{\infty}\phi_k(x)\delta u_k(t). \tag{13}$$

Substituting Eq. (13) into Eq. (12), we obtain

$$\sum_{j=1}^{\infty}\sum_{k=1}^{\infty} EI\int_0^L \phi_k''\phi_j''dx\ q_k(t)\delta u_j(t) + \sum_{j=1}^{\infty}\sum_{k=1}^{\infty}\rho A\int_0^L \phi_k\phi_j dx\ \ddot{q}_k(t)\delta u_j(t)$$
$$+\sum_{j=1}^{\infty}\sum_{k=1}^{\infty}\xi\int_0^L \phi_k\phi_j dx\ \dot{q}_k(t)\delta u_j(t)$$
$$=\sum_{j=1}^{\infty}\int_0^L p(x,t)\phi_j(x)dx\ \delta u_j(t) + \sum_{j=1}^{\infty}F(t)\phi_j(x_f)\delta u_j(t).$$

Therefore,

$$\sum_{j=1}^{\infty}\left(EI\int_0^L(\phi_j''(x))^2dx\ q_j(t) + \rho A\int_0^L \phi_j^2(x)dx\ \ddot{q}_j + \xi\phi_j^2(x)dx\ \dot{q}_j - p_j(t) - F_j(t)\right)\delta u_j(t) = 0,$$

where

$$p_j(t) := \int_0^L p(x,t)\phi_j(x)dx \text{ and } F_j(t) := \phi_j(x_f)F(t).$$

As $\delta u_j(t)$ is arbitrary, we have

$$m_j\ddot{q}_j(t) + c_j\dot{q}_j(t) + k_jq_j(t) = p_j(t) + F_j(t) \text{ for all } j = 1, 2, \ldots, \tag{14}$$

where the j^{th} modal mass, spring constant, and damping coefficient are defined as

$$m_j := \rho A\int_0^L \phi_j^2(x)dx,\ k_j := EI\int_0^L(\phi_j''(x))^2 \text{ and } c_j := \xi\int_0^L\phi_j^2(x)dx.$$

To obtain the necessary initial conditions of $q_j(t)$ for Eq. (14), we assume that

$$z(x,0) = a(x) \text{ and } \dot{z}(x,0) = b(x).$$

From Eq. (13), we have

$$a(x) = \sum_{k=1}^{\infty}\phi_k(x)q_k(0) \text{ and } b(x) = \sum_{k=1}^{\infty}\phi_k(x)\dot{q}_k(0).$$

Multiplying the above equations by $\phi_j(x)$ and integrating, we have the necessary conditions

$$q_j(0) = \frac{\rho A\int_0^L a(x)\phi_j(x)dx}{m_j} \text{ and } \dot{q}_j(0) = \frac{EI\int_0^L b(x)\phi_j(x)dx}{k_j}. \tag{15}$$

If the initial conditions are zero (that is $a(x) = b(x) = 0$) then $q_j(0) = \dot{q}_j(0) = 0$. Assuming zero initial conditions and taking the Fourier Transform of Eq. (14), we obtain Transform of $z(x,t)$ as

$$z(x,\omega) = \sum_{j=1}^{\infty}\frac{p_j(\omega) + F_j(\omega)}{-m_j\omega^2 + ic_j\omega + k_j}\phi_j(x). \tag{16}$$

Thus, we have obtained an expression of the cantilever displacement in terms of the forces on the cantilever. In the next section we only consider the first mode of vibration, i.e, the first term in the above summation.

2.2 Cantilever-Sample Interaction

If only the first mode of the multimode model presented in the earlier subsection is utilized then the cantilever-sample interaction can be modeled as shown in Figure 2. The cantilever is modeled as a single spring-mass system with the stiffness of the spring being $k = k_1$ and the equivalent mass $m = m_1$, where k_1 and m_1 are evaluated in the previous subsection. The cantilever interacts with the sample via a tip that is mounted on the cantilever. The cantilever-tip-sample system is modeled by a sphere of radius R and mass m, which is suspended by a spring of stiffness k. We will frequently refer to the mass m as being the tip of the cantilever.

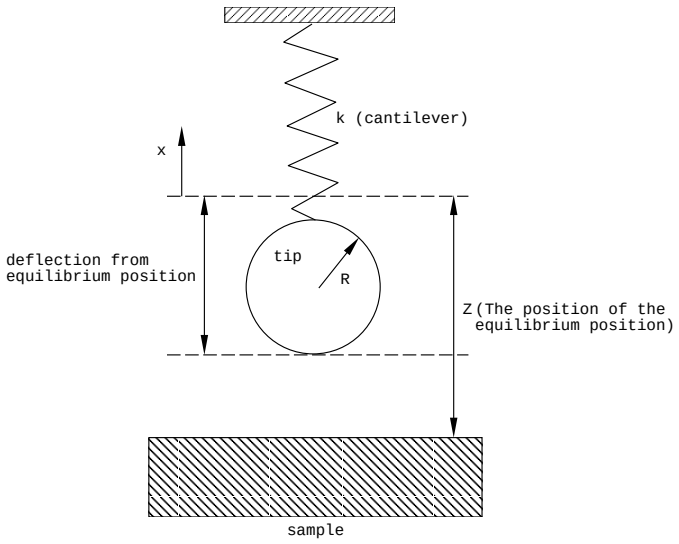

Figure 2: Tip-sample model

The tip-sample interaction is modeled by an interaction potential which is given by

$$-\frac{AR}{6(Z+x)},$$

where, Z is the equilibrium position of the tip measured from a reference where the sample is positioned in the absence of the sample, x is the displacement of the tip measured from this equilibrium position with the upward direction as the positive direction. $A = \pi^2 Q \rho_1 \rho_2$ is the Hamaker constant, where Q is the interaction constant (aqueous solute concentration in mole fraction units (mol dm^{-3}/55.5)) [9], and ρ_1 and ρ_2 are the densities of the tip and surface materials. Thus, the potential for the tip-sample assembly is given by

$$V(x, Z) = -\frac{AR}{6(Z+x)} + \frac{1}{2}kx^2.$$

The net energy of the system scaled by the effective mass m of the cantilever is given by

$H(x, \dot{x}, Z)$ with

$$H(x, \dot{x}, Z) = \frac{1}{2}\dot{x}^2 + \frac{1}{2}\omega_1^2 x^2 - \frac{D\omega_1^2}{(Z+x)},$$

where, $\omega_1 = \sqrt{\frac{k}{m}}$ is the first modal frequency of the system and $D = \frac{AR}{6k}$. Note that H is the Hamiltonian of the system, and therefore is a constant of the dynamics (invariant of motion) since there is no dissipation.

Let $x_1 = x$ and $x_2 = \dot{x}$. The dynamics of the tip-sample system derived from the above Hamiltonian is given below ($\dot{x}_1 = \frac{\partial H}{\partial x_2}$ and $\dot{x}_2 = -\frac{\partial H}{\partial x_1}$)

$$\dot{x}_1 = x_2 \tag{17}$$

$$\dot{x}_2 = -\omega_1^2 x_1 - \frac{D\omega_1^2}{(Z+x_1)^2}. \tag{18}$$

The actual system is both damped and forced, and therefore it is not Hamiltonian. We assume that the damping and external forcing are small enough so that we can think of the actual system as a perturbed Hamiltonian system. Hence, the study of the Hamiltonian (unperturbed) system is very important, as the trajectories of this system will be used (as we will see later) to study the behaviour of the perturbed system.

If $x > 0$ then the spring force and the vdW force both are directed towards the sample and therefore there will be no fixed points in this region. If $x < 0$ the spring force and the vdW force are directed in opposite directions and therefore there is a possibility of fixed points. The tip will not move if it is at a point where its velocity is zero and the spring force is equal to the vdW force in magnitude. If such a point exists, then it is called a fixed or equilibrium point. However, if Z is small enough, the system will not have fixed points because the vdW force will be larger than the spring force for $x < 0$. In this case, the surface snaps the tip into contact.

Next, we find the critical value of Z below which snapping occurs. We will also show that if Z is larger than this critical value then we have two fixed points above the surface.

At the fixed point the acceleration and the velocity of the tip must be equal to zero. Hence, to find the fixed points of the system we set $\dot{x}_1$ and $\dot{x}_2$ to zero in equations (17) and (18). $\dot{x}_1 = 0$ implies that $x_2 = 0$, and $\dot{x}_2 = 0$ gives

$$x_1^3 + Bx_1^2 + Cx_1 + D = 0, \tag{19}$$

where, $B = 2Z$ and $C = Z^2$. We will find the roots of this polynomial as a function of Z and D. Define

$$p = C - \frac{B^2}{3} = -\frac{Z^2}{3} \tag{20}$$

$$q = D - \frac{BC}{3} + \frac{2B^3}{27} = D - \frac{2Z^3}{27} \tag{21}$$

$$R_r = \frac{p^3}{27} + \frac{q^2}{4} = \left(\frac{D}{2}\right)^2 - \frac{1}{27}DZ^3. \tag{22}$$

Let $y^3 = -\frac{q}{2} \pm \sqrt{R_r}$ and the three cube roots of y^3 be $y_i, i = 1, 2, 3$. Then the three roots of (19); $x_{1i},\ i = 1, 2, 3$ are given by

$$x_{1i} = y_i - \frac{p}{3y_i} - \frac{B}{3},\ i = 1, 2, 3. \tag{23}$$

If $R_r < 0$ then y^3 is imaginary, otherwise it is real. Let Z_s be the solution to $R_r = 0$, i.e., the solution to

$$\left(\frac{D}{2}\right)^2 - \frac{1}{27} D Z_s^3 = 0,$$

which implies that

$$Z_s = \frac{3}{2}(2D)^{\frac{1}{3}}.$$

We divide the analysis of the dynamics into two cases; $Z \geq Z_s$ and $Z < Z_s$.

3 Dynamical Analysis: The Case $Z \geq Z_s$

In this section we discuss the important case when $Z \geq Z_s$, and at the end of the section we give a comment concerning the other case. First we analyze the system when there is no damping and forcing which will form the basis for the study of the perturbed system where the cantilever is forced sinusoidally and damping is present.

If $Z > Z_s$, $R_r < 0$ and y^3 is imaginary, we can write

$$y^3 = -\frac{q}{2} \pm j\sqrt{-R_r} = r^3 e^{\pm j\theta}, \tag{24}$$

where,

$$r^3 = \sqrt{\frac{q^2}{4} - R_r} \tag{25}$$

and

$$\theta = \arctan \frac{\sqrt{-R_r}}{-q/2}. \tag{26}$$

We consider only $+j\theta$ because (as we will see later) $-j\theta$ gives the same results. Thus, the three roots of y^3 are $y_i = re^{j\theta_i}$, where, $\theta_1 = \frac{\theta}{3},\ \theta_2 = \theta_1 + \frac{2\pi}{3},$ and $\theta_3 = \theta_1 + \frac{4\pi}{3}$. Therefore, we have

$$\begin{aligned} x_{1i} &= re^{j\theta_i} - \frac{p}{3r} e^{-j\theta_i} - \frac{B}{3} \\ &= r(\cos\theta_i + j\sin\theta_i) - \frac{p}{3r}(\cos\theta_i - j\sin\theta_i) - \frac{B}{3} \\ &= \left(r - \frac{p}{3r}\right)\cos\theta_i - \frac{B}{3} + j\sin\theta_i \left(r + \frac{p}{3r}\right), \end{aligned}$$

for $i = 1, 2, 3$. Note that

$$\begin{aligned} r^3 &= \sqrt{\frac{q^2}{4} - R_r} \\ &= \sqrt{-\frac{p^3}{27}} = \frac{Z^3}{27}. \end{aligned}$$

Therefore, $r = Z/3$ and we get

$$r + \frac{p}{3r} = \frac{Z}{3} - \frac{-Z^2/3}{Z} = 0 \ (Z > 0).$$

Thus, the roots of (19) are real for $Z > Z_s$ and they are given by

$$x_{1i} = -\frac{2Z}{3}(1 - \cos\theta_i). \tag{27}$$

Note that θ_i appears in the expression above only as $\cos\theta_i$ which is an even function of θ_i. Therefore, in (24) we can restrict the analysis to the roots of $y^3 = r^3 e^{j\theta}$. Thus, the fixed points for the system when $Z > Z_s$ are given by

$$(x_{1i}, 0), \ i = 1, 2, 3, \tag{28}$$

where, $x_{1i}, \ i = 1, 2, 3$ are given by (27).

At the fixed point, the vdW force $\frac{mD\omega_1^2}{(Z+x_1)^2}$ and the spring force kx_1 must be equal in magnitude and opposite in direction. In other words, for a fixed point to exist at $(x_1, 0)$ the following relation must hold

$$-kx_1 = \frac{mD\omega_1^2}{(Z + x_1)^2}.$$

In Figure 3 the vdW forces for $Z = Z_s, \ Z = Z_1 < Z_s, \ Z = Z_2 > Z_s,$ and Z = $Z_3 > Z_2$, and the spring force are plotted against x_1. The tip positions corresponding to the fixed points are the intersection points of the vdW and spring forces.

Note that when $Z = Z_s, \ R_r = 0$ and from equations (25) and (26) we have that $\theta = \pi$ (since $-q/2$ is negative in this case). Thus, $\theta_1 = \frac{\pi}{3}, \ \theta_2 = \pi,$ and $\theta_3 = \frac{5\pi}{3}$. Therefore, $x_{11} = -\frac{Z_S}{3}, \ x_{12} = -\frac{4Z_S}{3}$, and $x_{13} = -\frac{Z_S}{3}$. x_{11} and x_{13} are equal and are located above the surface. x_{12} lies below the surface and thus has no practical significance. The spring force is equal to the vdW force at only one point above the surface, namely $-Z_s/3$. This means that the spring force is the tangent of the vdW force at the point $-Z_s/3$ (see Figure 3).

If $Z > Z_s$ then it is clear that that $\theta \in (0, \pi)$. Therefore, $\theta_1 \in (0, \frac{\pi}{3}), \ \theta_2 \in (\frac{2\pi}{3}, \pi),$ and $\theta_3 \in (\frac{4\pi}{3}, \frac{5\pi}{3})$. This implies that $x_{11} \in (-Z_s/3, 0), \ x_{12} \in (-4Z/3, -Z),$ and $x_{13} \in (-Z, -Z_s/3)$. Thus, we have two fixed points above the surface. This is also clear from Figure 3. Note that as Z increases the points x_{11} and x_{13} move towards zero and the surface, respectively. The two roots that correspond to the equilibrium points that are located above the surface

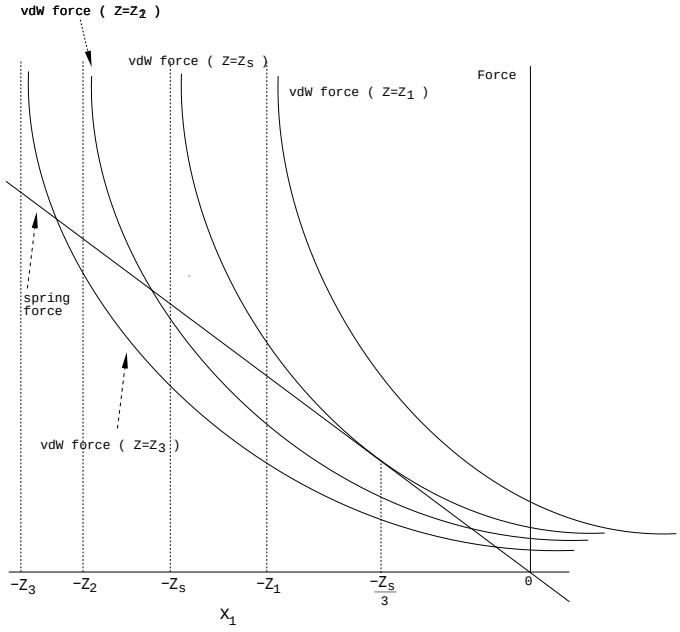

Figure 3: This figure shows the vdW force for different values of Z. The spring force is also plotted.

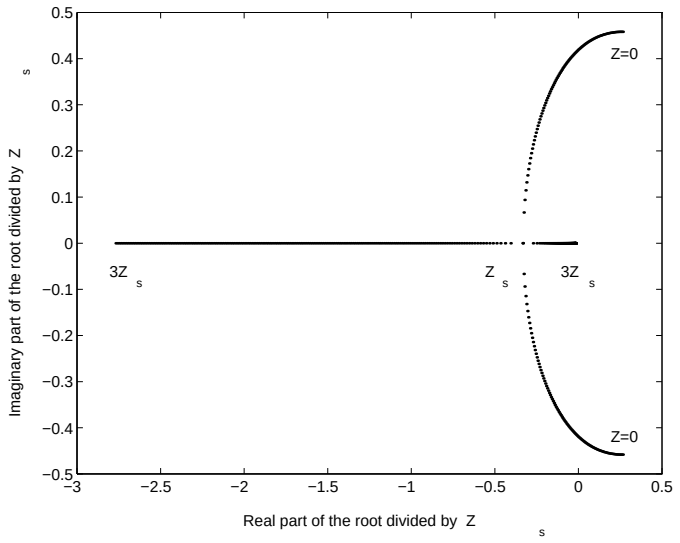

Figure 4: Root locus plot of the roots of (19) that correspond to the two fixed points above the surface as a function of Z

are plotted as a function of Z as shown in Figure 4. We can see that one equilibrium point moves towards zero and the other one towards the sample as Z increases.

As Z goes to ∞, θ goes to zero since $\frac{\sqrt{-R_r}}{-q/2}$ goes to zero with positive $-q/2$. Hence, x_{11} goes to zero, x_{12} goes to the surface from below, and x_{13} goes to the surface from above. There is a fixed point at zero because the vdW force is equal to zero there. Since Z goes to ∞, the spring force is larger than the vdW force at any point between the surface and $x_{11} = 0$. When the tip gets closer to the surface the vdW force increases rapidly and it becomes equal to the spring force at a point that approaches the surface (see Figure 3).

3.1 Phase Portrait

We will examine the nature of the fixed points by linearizing the system as given below

$$\begin{pmatrix} \dot{x}_1 \\ \dot{x}_2 \end{pmatrix} = \begin{pmatrix} 0 & 1 \\ -\omega_1^2 + \frac{2D\omega_1^2}{(Z+x_{1i})^3} & 0 \end{pmatrix} \begin{pmatrix} x_1 \\ x_2 \end{pmatrix}, \ i = 1, 3.$$

For $Z > Z_s$ the eigenvalues of the linearized system are purely imaginary at $x_1 = x_{11}$, and real with equal magnitude and opposite sign at $x_1 = x_{13}$. Thus, the fixed point x_{11} is a center, whereas x_{13} is a saddle point. From now on, we will denote x_{11} and x_{13} by x_c and x_s, respectively.

Figure 5 shows the phase portrait of the system. There is a homoclinic orbit connected to itself at the point $(x_s, 0)$. This homoclinic orbit is filled with periodic orbits around the the center $(x_c, 0)$. When $x_1 < x_s$ the tip accelerates towards the surface and hits it with a large velocity (snapping). Denote the maximum position on the x_1 axis that the homoclinic orbit obtains by x_e. If $x_s < x_1 < x_e$ and x_2 is not too large, the tip oscillates around the center. If x_2 is large enough, then the tip will have extra energy, so it will pass x_s accelerating towards the surface.

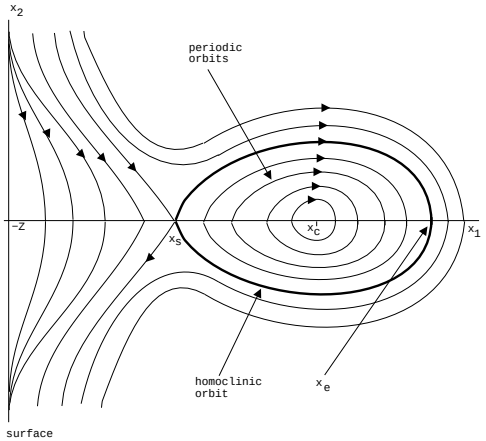

Figure 5: phase portrait

3.2 Homoclinic Solution

In this section, we find an analytic relation between time and x_1 for the homoclinic orbit. Since the Hamiltonian of the system is an invariant of motion, it is constant along the trajectories of the system. Thus, the homoclinic solution satisfies the following equation

$$H(x_1, x_2, Z) = H(x_s, 0, Z).$$

If we let $c = H(x_s, 0, Z)$, we have

$$\frac{1}{2}x_2^2 + \frac{1}{2}\omega_1^2 x_1^2 - \frac{D\omega_1^2}{(Z + x_1)} = c.$$

This can be written as

$$x_2^2 = -\omega_1^2 \frac{x_1^3 + Zx_1^2 - \frac{2c}{\omega_1^2}x_1 - 2\left(D + \frac{c}{\omega_1^2}Z\right)}{Z + x_1}. \tag{29}$$

The roots of the numerator of the right hand side of this expression are x_s (two repeated roots) and x_e. This is because the homoclinic orbit crosses the x_1 axis at the points x_s and x_e. Since for $H(x_1, x_2, Z) = c$, the solution exits on both sides of the saddle point (since x_s has stable and unstable manifolds), x_s has to be a repeated root so that x_2^2 is positive around x_s. Therefore, we have

$$\begin{aligned} & x_1^3 + Zx_1^2 - \frac{2c}{\omega_1^2}x_1 - 2\left(D + \frac{c}{\omega_1^2}Z\right) = (x_1 - x_s)^2 (x_1 - x_e) \\ = \;& x_1^3 - (x_e + 2x_s)\, x_1^2 + \left(2x_s x_e + x_s^2\right) x_1 - x_s^2 x_e. \end{aligned} \tag{30}$$

Equating the coefficients of x_1^2 in (30) we have, $Z = -(x_e + 2x_s)$. Solving for x_e, we get

$$x_e = -Z - 2x_s = -x_s - (Z + x_s). \tag{31}$$

Using (19) and (31) it is easy to show that the other coefficients in (30) are equal which justifies our claim.

Note that x_e is equal to the difference between the two dimensions that are shown in Figure 6. From equation (29) we have

$$x_2 = \pm\omega_1 (x_1 - x_s) \sqrt{\frac{x_e - x_1}{Z + x_1}}, \;\; (x_s \le x_1 \le x_e).$$

To obtain the homoclinic orbit we will solve the equations of motion and assume that the time origin t_0 is chosen so that $x_1(t_0) = x_e$. It is clear that if $t \ge t_0$ then the trajectory is such that $x_2(t) \le 0$. Therefore, we have for $t \ge t_0$

$$\dot{x}_1 = x_2 = -\omega_1 (x_1 - x_s) \sqrt{\frac{x_e - x_1}{Z + x_1}}, \;\; (x_s \le x_1 \le x_e). \tag{32}$$

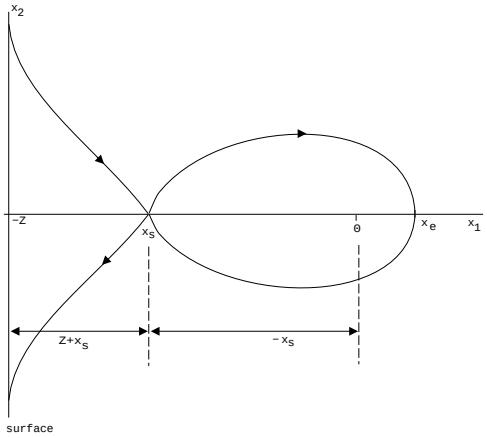

Figure 6: Homoclinic orbit

(Note that the right hand side is always negative in the region of interest). Similarly, if $t < t_0$ then $x_2 > 0$ and we have

$$\dot{x}_1 = x_2 = +\omega_1 (x_1 - x_s) \sqrt{\frac{x_e - x_1}{Z + x_1}}, \ (x_s \leq x_1 \leq x_e). \tag{33}$$

We will now solve for $x_1(t)$ when $t \geq t_0$. Separation of variables in equation (32) yields

$$\frac{1}{x_1 - x_s} \sqrt{\frac{Z + x_1}{x_e - x_1}} dx_1 = -\omega_1 dt. \tag{34}$$

Substituting $u = x_1 - x_s$ in (34), we have

$$\frac{1}{\sqrt{P}} du + \frac{Z + x_s}{u\sqrt{P}} du = -\omega_1 dt, \tag{35}$$

where, $P = [(Z + x_s) + u]\,[(x_e - x_s) - u]$. Note that when $t = t_0$, $u = x_e - x_s$. Integrating (35) from time t_0 to time t and substituting back $x_1 = u + x_s$, we have (see [8])

$$\begin{aligned} &- \arcsin \frac{x_1 + Z + x_s}{x_s} - \sqrt{\frac{Z + x_s}{-Z - 3x_s}} * \\ &\ln - \left(\frac{(Z + x_s)(-Z - 3x_s) + (-Z - 2x_s)(x_1 - x_s) + \sqrt{(Z + x_s)(x_e - x_s) P}}{x_s (x_1 - x_s)} \right) \\ &- \frac{\pi}{2} = -\omega_1 (t - t_0), \end{aligned} \tag{36}$$

where, (as we had earlier) $x_s = -\frac{2Z}{3}(1 - \cos\theta_3)$. Therefore, if the initial condition at time t_0 for the system is $(x_e, 0)$ then for $t \geq t_0$, $x_1(t)$ is obtained from equation (36) and

$$x_2 = -\omega_1 (x_1 - x_s) \sqrt{\frac{x_e - x_1}{Z + x_1}}. \tag{37}$$

Similarily, if the initial condition at time t_0 for the system is $(x_e, 0)$ then for $t < t_0$, $x_1(t)$ is obtained from the following equation

$$
\begin{aligned}
&-\arcsin\frac{x_1+Z+x_s}{x_s}-\sqrt{\frac{Z+x_s}{-Z-3x_s}}\,*\\
&\ln-\left(\frac{(Z+x_s)(-Z-3x_s)+(-Z-2x_s)(x_1-x_s)+\sqrt{(Z+x_s)(x_e-x_s)P}}{x_s(x_1-x_s)}\right)\\
&-\frac{\pi}{2}=+\omega_1(t-t_0),
\end{aligned}
\tag{38}
$$

and $x_2(t)$ is obtained from

$$
x_2=+\omega_1(x_1-x_s)\sqrt{\frac{x_e-x_1}{Z+x_1}}. \tag{39}
$$

Note that for a given x_1 in the desired range of interest $x_2(-\tau)=-x_2(\tau)$ for $\tau=t-t_0$. Therefore, x_2 is an odd function of τ. Thus, we have obtained a complete description of the homoclinic orbit.

3.3 The Perturbed System

In most AFMs the cantilever motion is damped due to the surrounding air. In addition, the cantilever is forced by a small sinusoidal signal $mf\cos\omega t$, where, ω takes values around the natural frequency ω_1 of the system. The differential equation for the perturbed system can be written as

$$
\begin{aligned}
\dot{x}_1 &= x_2\\
\dot{x}_2 &= -\omega_1^2 x_1-\frac{D\omega_1^2}{(Z+x)^2}+f\cos\omega t-\mu x_2,
\end{aligned}
$$

where we have assumed that the damping force per unit mass is μx_2. Given a small enough ϵ (what we mean by small enough will become clear later), define γ and δ such that $\epsilon\gamma=f$ and $\epsilon\delta=\mu$. Using suspension (i.e, consider the time to be a new state variable, ϕ), we have

$$
\begin{aligned}
\dot{x}_1 &= x_2\\
\dot{x}_2 &= -\omega_1^2 x_1-\frac{D\omega_1^2}{(Z+x)^2}+\epsilon(\gamma\cos\phi-\delta x_2)\\
\dot{\phi} &= \omega,
\end{aligned}
$$

where $\phi(t)=\omega t+t_0$. Define

$$
g(x_1,x_2,\phi)=\begin{pmatrix}0\\ \gamma\cos\phi-\delta x_2\end{pmatrix}.
$$

Thus, the Hamiltonian system described previously is now perturbed by ϵg. The next step is to study the dynamics of the perturbed system. To achieve this goal, we will study the Melnikov function for the perturbed system.

3.4 Melnikov Function

Since the system that we are considering is a time-periodic perturbation of a Hamiltonian system, Melnikov's method can be used to describe how the homoclinic orbit breaks up in the presence of the perturbation. The Melnikov function is defined as [1]

$$M(t_0, \phi_0) = \int_{-\infty}^{\infty} DH(x_{1h}(\tau), x_{2h}(\tau)) g(x_{1h}(\tau), x_{2h}(\tau), \phi(\tau + t_0)) d\tau,$$

where, $DH(x_1, x_2) = \left(\frac{\partial H}{\partial x_1} \quad \frac{\partial H}{\partial x_2}\right)$, and $x_{1h}(\tau)$ and $x_{2h}(\tau)$ are the homoclinic solution as given by equations (36), (37), (38), and (39). Therefore,

$$\begin{aligned} M(t_0, \phi_0) &= \int_{-\infty}^{\infty} x_{2h}(\tau) \left(\gamma \cos(\omega\tau + \omega t_0 + \phi_0) - \delta x_{2h}(\tau)\right) d\tau \\ &= -\delta \int_{-\infty}^{\infty} x_{2h}^2(\tau) d\tau + \gamma \cos(\omega t_0 + \phi_0) \int_{-\infty}^{\infty} x_{2h}(\tau) \cos \omega\tau d\tau \\ &\quad -\gamma \sin(\omega t_0 + \phi_0) \int_{-\infty}^{\infty} x_{2h}(\tau) \sin \omega\tau d\tau \\ &= -2\delta \int_{0}^{\infty} x_{2h}^2(\tau) d\tau - 2\gamma \sin(\omega t_0 + \phi_0) \int_{0}^{\infty} x_{2h}(\tau) \sin \omega\tau d\tau. \end{aligned}$$

The last equality holds because $x_{2h}(\tau)$ is an odd function of τ, assuming $x_{1h} = x_e$ at $t = t_0$. Let $a_d = -2\int_0^\infty x_{2h}^2(\tau) d\tau$ and $a_s = -2\int_0^\infty x_{2h}(\tau) \sin \omega\tau d\tau$. Hence,

$$M(t_0, \phi_0) = a_d \delta + a_s \gamma \sin(\omega t_0 + \phi_0). \tag{40}$$

The Melnikov function is a signed measure of the distance between the stable and unstable manifolds for the perturbed system. The manifolds intersect if the Melnikov function has zeros. The intersection of manifolds indicates the presence of chaos [1]. The Melnikov function will have zeros if and only if

$$\frac{\delta}{\gamma} \leq \left| \frac{a_s}{a_d} \right|.$$

Define

$$\left(\frac{\delta}{\gamma}\right)_{cr} = \left| \frac{a_s}{a_d} \right|.$$

If $\frac{\delta}{\gamma} > \left(\frac{\delta}{\gamma}\right)_{cr}$ then $M(t_0, \phi_0)$ has no zeros, otherwise it does.

ϕ_0 fixes a Poincaré section, while t_0 specifies a point on the unperturbed homoclinic orbit. Every zero of the Melnikov function corresponds to an intersection (within order ϵ) of the stable and unstable manifolds [1, 2]. Note that if $\frac{\delta}{\gamma} \leq \left(\frac{\delta}{\gamma}\right)_{cr}$ then the two manifolds intersect at an infinite number of points for every Poincaré section ϕ_0.

3.5 Qualitative Behaviour

In this subsection, we define variables which facilitate the study of the qualitative behaviour of the system. Recall that

$$\begin{aligned} \dot{x}_1 &= x_2 \\ \dot{x}_2 &= -\omega_1^2 x_1 - \frac{D\omega_1^2}{(Z+x_1)^2} + \epsilon\left(\gamma\cos\omega t - \delta x_2\right). \end{aligned}$$

Let $T = \omega_1 t$ (time scale) and divide the left and right hand sides of the above equations by Z_s to get

$$\begin{aligned} \xi_1' &= \xi_2 \\ \xi_2' &= -\xi_1 - \frac{d}{(\alpha+\xi_1)^2} + \epsilon\left(\Gamma\cos\Omega T - \Delta\xi_2\right), \end{aligned}$$

where, $\xi_1 = \frac{x_1}{Z_s}$, $\xi_2 = \frac{x_2}{\omega_1 Z_s}$, $d = \frac{4}{27}$, $\Gamma = \frac{\gamma}{\omega_1^2 Z_s}$, $\Delta = \frac{\delta}{\omega_1}$, $\alpha = \frac{Z}{Z_s}$, and $\Omega = \frac{\omega}{\omega_1}$. The prime denotes the derivative with respect to T. In the new co-ordinates there is no explicit dependence on D and ω_1 (note that the same γ and δ give different Γ and Δ for different values of D and ω_1). In other words, there is no explicit dependence on the material properties and the dimensions of the cantilever and tip. The quantitative results differ by scaling factors depending on these two parameters.

The new system looks like the old system with Z replaced by α, D by d and ω_1 by 1. Hence, all of the previous analysis applies to the new system with the new factors. The Melnikov function in the new co-ordinates is

$$M(T_0, \phi_0) = A_d\Delta + A_s\Gamma\sin(\Omega T_0 + \phi_0),$$

where, $A_d = -2\int_0^\infty \xi_{2h}^2(\tau)d\tau$, and $A_s = -2\int_0^\infty \xi_{2h}(\tau)\sin\Omega\tau d\tau$. Define the critical value of $\frac{\Delta}{\Gamma}$ as $\left(\frac{\Delta}{\Gamma}\right)_{cr} = \left|\frac{A_s}{Ad}\right|$. It is easy to verify that

$$\left(\frac{\delta}{\gamma}\right)_{cr} = \frac{1}{\omega_1 Z_s}\left(\frac{\Delta}{\Gamma}\right)_{cr}.$$

$\left(\frac{\Delta}{\Gamma}\right)_{cr}$ is computed numerically for different values of $\alpha > 1$ and Ω around 1. The results are plotted as shown in Figure 7. If the material properties and dimensions of the cantilever and tip are given, then we first compute Z_s and ω_1 and then with the appropriate scaling transform Figure 7 to a figure with $\frac{\delta}{\gamma}$, Z, and ω as co-ordinates.

Intersection of the stable and the unstable manifolds occurs for points which lie below the surface plotted in Figure 7. As α increases the system tends to the spring-mass-damper system behaviour which does not exhibit chaotic motion when it is perturbed by a sinusoidal external forcing, and the exact trajectories of the system can be found analytically. When Z is small enough,i.e., α is close enough to 1, again there will be no chaotic motion because x_s and x_e get close enough to each other such that small perturbations cause the motion to be outside the homoclinic orbit and the surface will snap the tip into contact. If we fix α then as Ω increases the chance for chaos decreases.

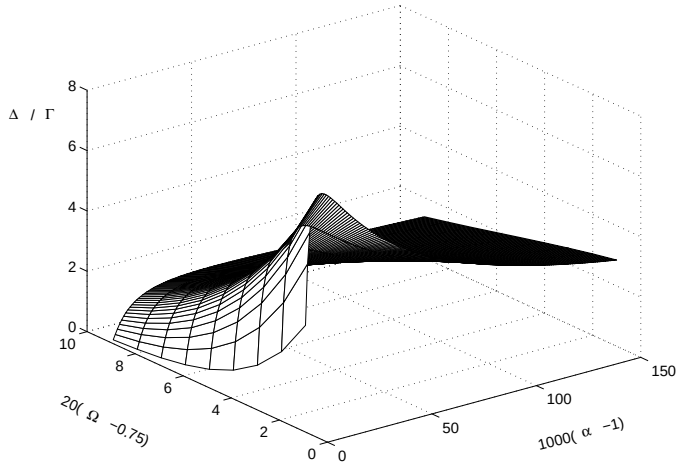

Figure 7: $\left(\frac{\Delta}{\Gamma}\right)_{cr}$ surface. The region below the surface is the region where chaos exists in the system. The region above the surface is the region of no chaos.

3.6 State Feedback Control

In most AFMs the state x_1 (position) is measured, and the state x_2 (velocity) can be estimated. This makes it possible to apply a force of the form $u = k_p x_1 + k_v x_2$ to the cantilever. In this case, the state equations of the system are written as

$$\begin{aligned}
\dot{x}_1 &= x_2 \\
\dot{x}_2 &= -\omega_1^2 x_1 - \frac{D\omega_1^2}{(Z+x_1)^2} + \epsilon\left(\gamma\cos\omega t - \delta x_2\right) + \frac{k_p}{m}x_1 + \frac{k_v}{m}x_2 \\
&= -\omega_{n1}^2 x_1 - \frac{D_1\omega_{n1}^2}{(Z+x_1)^2} + \epsilon\left(\gamma\cos\omega t - \delta_1 x_2\right),
\end{aligned}$$

where, $(\omega_{n1})^2 = \frac{k_1}{m}$ with $k_1 = k - k_p$, $D_1 = \frac{AR}{6k_1}$, and $\delta_1 = \delta - \frac{1}{\epsilon}\frac{k_v}{m}$.

We can see that applying the above state feedback control is equivalent to changing k and δ in the system independently. Note that $k_1 = 0$ means that the tip accelerates towards the sample regardless of the initial condition. If $k_1 < 0$ there is only one equilibrium point above the sample $(x_1 > 0, 0)$ which is unstable. We will restrict our analysis to the case when $k_1 > 0$ and $\delta_1 \geq 0$.

Since k_1 and δ_1 are independent, we will discuss the effect of changing each one separately. We assume that ω, γ and Z are fixed. Suppose that $k_2 > k_1 > 0$. Then it is easy to see from Figure 8 that $-Z < x_{s2} < x_{s1}$, $0 > x_{c2} > x_{c1}$ and $Z_{s2} < Z_{s1}$. A stiffer spring allows the tip to get closer to the sample before snapping occurs, and it shifts x_c closer to zero. The homoclinic orbits for k_1 and k_2 are shown in Figure 9. It is clear that the homoclinic orbits for k_1 and k_2 do not intersect.

Now by fixing $k = k_0$ and $\delta = \delta_0$ we get the point $(\alpha_0,\ \Omega_0,\ \left(\frac{\Delta}{\Gamma}\right)_0)$ in a three dimensional

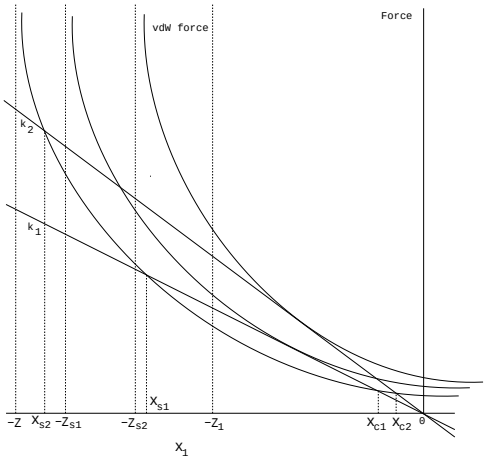

Figure 8: Spring and vdW forces.

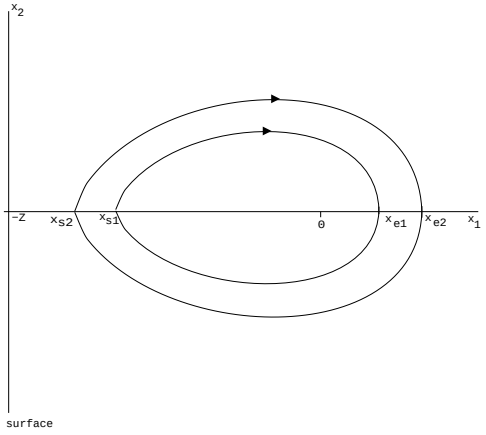

Figure 9: Homoclinic orbits for $k_2 > k_1$

space, where $\alpha_0 = \frac{Z}{Z_{s0}}$ with $Z_{s0} = \frac{3}{2}\left(2\frac{AR}{6k_0}\right)^{\frac{1}{3}}$, $\Omega_0 = \frac{\omega}{\omega_{10}}$ with $\omega_{10} = \sqrt{\frac{k_0}{m}}$, and $\left(\frac{\Delta}{\Gamma}\right)_0 = \omega_{10} Z_{s0} \frac{\delta_0}{\gamma}$. Let $k = \rho k_0$, where $\rho > 0$. It is easy to see that this corresponds to the point $(\rho^{\frac{1}{3}}\alpha_0,\ \rho^{\frac{-1}{2}}\Omega_0,\ \rho^{\frac{1}{6}}\left(\frac{\Delta}{\Gamma}\right)_0)$. Varying ρ is equivalent to varying k. The variation of ρ induces a variation of the point $(\rho^{\frac{1}{3}}\alpha_0,\ \rho^{\frac{-1}{2}}\Omega_0,\ \rho^{\frac{1}{6}}\left(\frac{\Delta}{\Gamma}\right)_0)$ on a one dimensional curve in a three dimensional space. Each curve is characterized by a fixed ω, γ, Z, and δ, and each point on the curve corresponds to a particular k. As k increases the point moves in the $+\alpha$, $-\Omega$, $+\frac{\Delta}{\Gamma}$ direction, and vice versa. Figures 10 and 11 show curves of constant ω, γ, Z, and δ along with the $\left(\frac{\Delta}{\Gamma}\right)_{cr}$ surface. Recall that when the operating point is on or under this surface the stable and unstable manifolds intersect, otherwise they do not. If the curve of constant ω, γ, Z, and δ intersects the $\left(\frac{\Delta}{\Gamma}\right)_{cr}$ surface, then we can move the operating point from one side of this surface to the other by changing k appropriately. Note that by varying k the $\left(\frac{\delta}{\gamma}\right)_{cr}$ surface shifts in the Z, ω and $\frac{\delta}{\gamma}$ co-ordinates , while it is fixed in the α, Ω and $\frac{\Delta}{\Gamma}$ co-ordinates. Clearly, with the aid of this diagram we can select the controller parameter k_p to suppress the possibility of chaos.

Now we will analyze the effect of the controller term k_v. Let $k = k_0$ be a fixed constant and let $\delta = \rho\delta_0$. These nominal conditions give the point $(\alpha_0,\ \Omega_0,\ \rho\left(\frac{\Delta}{\Gamma}\right)_0)$. By varying ρ (δ) the operating point moves in the vertical $(\frac{\Delta}{\Gamma})$ direction . As δ increases the operating point moves in the $+\frac{\Delta}{\Gamma}$, and vice versa. Thus, we can move the operating point from one side of the $\left(\frac{\Delta}{\Gamma}\right)_{cr}$ surface to the other by changing δ appropriately. This procedure gives us the controller term k_v which results in the elimination of the possibility of chaos.

In summary, the tools of Melnikov theory are used to provide a procedure for the design of a controller of the form $u = k_v x_1 + k_p x_2$ that will eliminate chaos if it exists when $u = 0$.

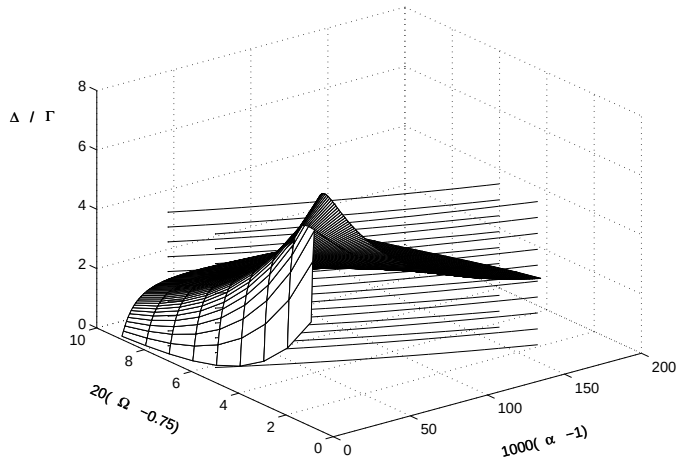

Figure 10: lines of constant ω, γ, Z, and δ and the $\left(\frac{\Delta}{\Gamma}\right)_{cr}$ surface

Finally, for the case when $Z = Z_1 < Z_s$, the vdW force is greater than the spring force

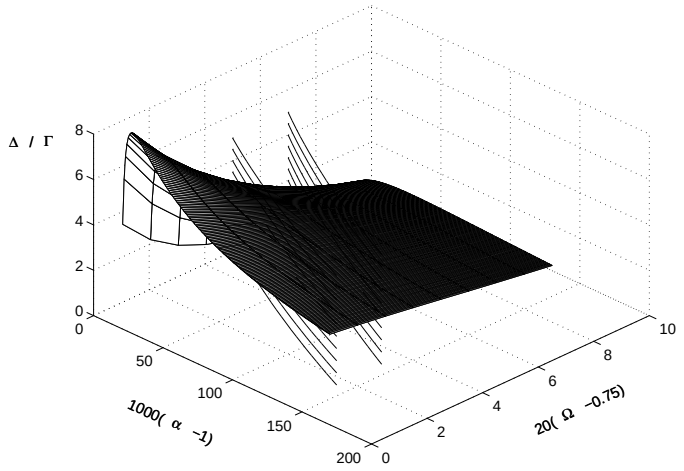

Figure 11: lines of constant ω, γ, Z, and δ and the $\left(\frac{\Delta}{\Gamma}\right)_{cr}$ surface

whenever $x_1 < 0$ (see Figure 3). Hence, there are no fixed points above the surface and the corresponding two roots are imaginary as shown in Figure 4. In this case, the surface snaps the tip into contact.

4 Conclusions

A mathematical model for the cantilever-sample interaction in the AFM was utilized to explore the dynamical behaviour of the cantilever. It is shown that it is possible for chaos to exist in the system depending on the extent of damping and forcing. The region in which chaos exists was found. It was shown that feedback control can be used to eliminate the possibility of chaos. Ongoing research involves the experimental validation of the predictions, and the implementation of control to eliminate chaos.

References

[1] Stephen Wiggins, Introduction to Applied Nonlinear Dynamical Systems and Chaos, Springer-Verlag, 1990.

[2] Stephen Wiggins, Chaotic Transport in Dynamical Systems, Springer-Verlag, 1992.

[3] M. V. Salapaka, H. S. Bergh, J. Lai, A. Majumdar, and E. McFarland, "Multimode Noise Analysis of Cantilevers for Scanning Force Microscopy", to appear.

[4] H.J. Butt, and M. Jaschke, Nanotechnology, **6**(1), 1-7 (1995).

[5] R. R. Craig, *Structural Dynamics, An Introduction to Computer Methods*, John Wiley and Sons, New York, 1981.

[6] Jeffrey L.Hutter and John Bechhoefer, "Calibration of atomic-force microscope tips", *Rev. Sci. Instrum.* 64(7), pp. 1868-1873, July 1993.

[7] Maurice I. Young, Structural Dynamics and Vibrations of Damped Aircraft-Type Structure, NASA Contractor Report 4424, 1992.

[8] I. S. Gradshteyn/I. M. Ryzhik, Table of Integrals, Series, and Products, Academic Press, Inc., 1980.

[9] Jacob N. Israelachvili, Intermolecular and Surface Forces, Academic Press, 1985.

[10] Dror Sarid, *Scanning Force Microscopy,* Oxford University Press, New York, 1994.

[11] N. A. Burnham, A. J. Kulik, G. Gremaud, and G. A. D. Briggs, "Nanosubharmonics: The Dynamics of Small Nonlinear Contacts", *Physical Rev. Lett.* , Vol. 74, pp 5092-5059, June 1995.